Available online at www.sciencedirect.com
ScienceDirect
International Journal of Heat and Mass Transfer 50 (2007) 3925–3932
International Journal of HEAT and MASS TRANSFER
www.elsevier.com/locate/ijhmt

A fractal resistance model for flow through porous media

Jinsui Wu [a,b], Boming Yu [a,*]

[a] Department of Physics, Huazhong University of Science and Technology, 1037 Luoyu Road, Wuhan 430074, PR China
[b] Department of Physics, North China Institute of Science and Technology, Yanjiao Town, Sanhe City, Hebei 06520, PR China

Received 19 September 2006; received in revised form 25 January 2007
Available online 5 April 2007

Abstract

A fractal model for resistance of flow through porous media is developed based on the fractal characters of porous media and on the pore–throat model for capillary. The proposed model is expressed as a function of the pore–throat ratio, porosity, property of fluid, pore/capillary and particle sizes, fluid velocity (or Reynolds number) and fractal dimensions of porous media. There is no empirical constant and every parameter has clear physical meaning in the proposed model. The model predictions are compared with experiment data, and good agreement is found between them.

Keywords: Porous media; Fractal; Flow resistance; Laminar flow

1. Introduction

The widely employed resistance model for flow through porous media was proposed by Ergun [1] in 1952. This model is called Ergun equation:

$$\frac{\Delta P}{L_0} = \frac{150\mu(1-\varepsilon)^2 v_s}{D_p^2 \varepsilon^3} + 1.75\frac{1-\varepsilon}{\varepsilon^3}\frac{\rho v_s^2}{D_p} \quad (1)$$

where ΔP is the pressure drop, L_0 is the length along the macroscopic pressure gradient in porous media, v_s is the superficial velocity (defined by $v_s = Q/A$, where Q is the total flow rate through a cross section of area A), μ is the absolute viscosity of fluid, ε is the porosity, and D_p is the appropriate characteristic length for a medium or the equivalent mean diameter of particles, ρ is the density of fluid. Eq. (1) is based on the average hydraulic radius [2]. The first term on the right side of Eq. (1) is called Blake-Kozeny equation, i.e. $\frac{\Delta P}{L_0} = \frac{150\mu(1-\varepsilon)^2 v_s}{D_p^2 \varepsilon^3}$, which represents the viscous energy loss primarily in laminar flow, and pressure drop for flow at low speed (or low Reynolds number) is mainly determined by the viscous energy loss, i.e. when the modified Reynolds number ($Re_p = (D_p \rho v_s/\mu)(1-\varepsilon)^{-1}$) is less than 10 [2]. If the first term on the right side of Eq. (1) is neglected, Eq. (1) is reduced to $\frac{\Delta P}{L_0} = 1.75\frac{1-\varepsilon}{\varepsilon^3}\frac{\rho v_s^2}{D_p}$, which is called Burke-Plummer equation. Burke-Plummer equation denotes the kinetic energy loss primarily in turbulent flow and the kinetic/local energy loss dominates the pressure drop when the modified Reynolds number Re_p is higher than 100 [2]. The interior mechanism for the kinetic energy loss is not well understood. Ergun equation indicates that the pressure drop across the packing length is dependent upon the flow rate, the viscosity and density of fluid, and the size, shape and surface of packing materials [1]. It has been shown that the pressure loss as indicated by Eq. (1) is obtained by adding the viscous and kinetic energy losses. Ergun equation has been hotly debated in the past decades. Many investigators [3–10] discussed its applicability and different empirical constants under different porosities and particles.

It has been shown that the fractal geometry theory [11] has been used as a tool in many disciplines to characterize irregular or disordered objects [11–13] such as coast lines, clouds and islands, roughness of surfaces [14–16], sandstone pores [17,18], fracture surfaces of metal [19], and granular materials [20], etc. The pores and their distributions in porous media are analogous to islands or lakes

* Corresponding author. Tel.: +86 27 87542153; fax: +86 27 87543882.
E-mail address: yuboming2003@yahoo.com.cn (B. Yu).

0017-9310/$ - see front matter © 2007 Elsevier Ltd. All rights reserved.
doi:10.1016/j.ijheatmasstransfer.2007.02.009

on earth and to contact spots on engineering surfaces. Therefore, it is possible to model the transport properties such as flow resistance and permeability for flow in porous media by fractal geometry theory. In the light of this point, Yu et al. [21,22] proposed a fractal geometry model for permeability of porous media and their model has been shown to be suitable not only for particle porous media [21] but also for porous fabrics [22]. Their model is analytically expressed as a function of fractal dimensions (for pore spaces and for tortuous capillaries/streamlines) and microstructural parameters of the media. Karacan and Halleck [23] extended Yu and Cheng's [21] model to the prediction of the permeability for grain fragments. Recently, Shi et al. [24,25] extended Yu et al.'s fractal permeability model [21,22] to modeling the permeability for the gas diffusion layer (GDL) of PEM fuel cells, whose pore size is in the order of 10^{-5}–10^{-8} m. Meng et al. [26] also applied the fractal geometry theory to model the permeation of membrane fouling in membrane bioreactor. The cake layer formed on membrane surface presents a major challenge to membrane permeation, and it can be considered as a porous media. The cake layer permeability was derived and found to be a function of the pore-area fractal dimension and microstructural parameters.

From the above brief review, it is seen that the wide applications of the fractal geometry theory in many fields have been found. It, therefore, may be possible to develop the analytical model for resistance of flow in porous media based on the fractal geometry theory. In this paper, we derive a fractal model for resistance of flow through porous media with particles of different shapes based on the fractal characters of the media and on the pore–throat model for capillary. In the following section, the fractal characters of porous media are addressed first.

2. Fractal characters of porous media

It has been shown that the cumulative size distribution of pores in porous media follows the fractal scaling law [21,22]:

$$N(L \geqslant \lambda) = (\lambda_{\max}/\lambda)^{D_f} \tag{2}$$

where λ is the diameter of pores, $\lambda_{\max}$ is the maximum diameter of pores, N is the cumulative population of pores whose sizes are greater than or equal to λ, and D_f is the fractal dimension for pores, with $1 < D_f < 2$ in two dimensions and $2 < D_f < 3$ in three dimensions.

It is evident that the total number of pores, from the smallest diameter to the largest diameter, can be obtained from Eq. (2) as

$$N_t(L \geqslant \lambda_{\min}) = (\lambda_{\max}/\lambda_{\min})^{D_f} \tag{3}$$

Differentiating on both sides of Eq. (2) results in

$$-\mathrm{d}N = D_f \lambda_{\max}^{D_f} \lambda^{-(D_f+1)}\,\mathrm{d}\lambda \tag{4}$$

Dividing Eq. (4) by (3) yields

$$-\frac{\mathrm{d}N}{N_t} = D_f \lambda_{\min}^{D_f} \lambda^{-(D_f+1)}\,\mathrm{d}\lambda = f(\lambda)\,\mathrm{d}\lambda \tag{5}$$

where $f(\lambda) = D_f \lambda_{\min}^{D_f} \lambda^{-(D_f+1)}$ is the probability density function. The probability density function $f(\lambda)$ should satisfy the following normalization relation:

$$\int_{\lambda_{\min}}^{\lambda_{\max}} f(\lambda)\,\mathrm{d}\lambda = 1 - \left(\frac{\lambda_{\min}}{\lambda_{\max}}\right)^{D_f} = 1 \tag{6}$$

As a result, Eq. (6) holds if and only if [27]

$$(\lambda_{\min}/\lambda_{\max})^{D_f} = 0 \tag{7}$$

In general, $\lambda_{\min}/\lambda_{\max} \leqslant 10^{-2}$ in porous media, and Eq. (7) holds approximately, thus the fractal geometry theory and technique can be used to analyze properties of porous media. In above equations, fractal dimension D_f is given by [27]

$$D_f = d_E - \frac{\ln \varepsilon}{\ln(\lambda_{\min}/\lambda_{\max})} \tag{8}$$

where d_E is the Euclidean dimension, and $d_E = 2$ (3) in two (three) dimensions.

If one is interested in fractal particles, the above parameters and equations are immediately applicable as long as appropriate changes are made, for example, changing the porosity ε into the particle volume fraction, and pore diameter λ into the particle diameter, etc.

The tortuous capillaries have also been shown to follow the fractal scaling law given by [21]

$$L_t(\lambda) = \lambda^{1-D_T} L_0^{D_T} \tag{9}$$

where D_T is the fractal dimension for tortuous capillaries with $1 < D_T < 2$ in two dimensions, representing the convoluted extent of capillary pathways for fluid flow through a porous medium, and $L_t(\lambda)$ is the tortuous/real length. Due to the tortuous nature of the pore channel, $L_t(\lambda) \geqslant L_0$, where L_0 is the length along the macroscopic pressure gradient in the medium. Note that $D_T = 1$ represents a straight capillary path, and a higher value of D_T corresponds to a highly tortuous capillary.

Based on the above fractal characters of pores and tortuous capillaries in porous media, a fractal model for resistance of flow in porous media is derived in the following section.

3. Fractal model for flow resistances

3.1. The viscous energy loss along the flow path at low Reynolds numbers

In this model, we assume that a porous medium is comprised of a bundle of tortuous capillaries. The flow rate through a tortuous capillary is given by modifying the well known Hagen–Poiseulle equation as [28]

$$q(\lambda) = \frac{\pi}{128}\frac{\Delta P_1}{L_t}\frac{\lambda^4}{\mu} \tag{10}$$

The total flow rate Q through a unit cell can be obtained by integrating the individual flow rate, $q(\lambda)$, over the entire range of pores/capillaries from the minimum pore size $\lambda_{\min}$ to the maximum pore size $\lambda_{\max}$. According to Eqs. (4), (9) and (10), we have [21]

$$Q = -\int_{\lambda_{\min}}^{\lambda_{\max}} q(\lambda)\,\mathrm{d}N(\lambda) = \frac{\pi}{128\mu}\frac{\Delta p_1}{L_0}\frac{D_\mathrm{f}}{3+D_\mathrm{T}-D_\mathrm{f}}L_0^{1-D_\mathrm{T}}\lambda_{\max}^{3+D_\mathrm{T}} \tag{11}$$

The total pore area A_p is related to the total cross area A by $A = A_\mathrm{p}/\varepsilon$. The total pore area A_p can be obtained by

$$A_\mathrm{p} = -\int_{\lambda_{\min}}^{\lambda_{\max}} \frac{\pi\lambda^2}{4}\,\mathrm{d}N = \frac{\pi D_\mathrm{f}}{4(2-D_\mathrm{f})}\lambda_{\max}^2\left[1-\left(\frac{\lambda_{\min}}{\lambda_{\max}}\right)^{2-D_\mathrm{f}}\right] \tag{12}$$

Thus, the total cross area A is

$$A = \frac{A_\mathrm{p}}{\varepsilon} = \frac{\pi D_\mathrm{f}}{4\varepsilon(2-D_\mathrm{f})}\lambda_{\max}^2\left[1-\left(\frac{\lambda_{\min}}{\lambda_{\max}}\right)^{2-D_\mathrm{f}}\right] \tag{13}$$

Due to [27]

$$\varepsilon = \left(\frac{\lambda_{\min}}{\lambda_{\max}}\right)^{2-D_\mathrm{f}} \tag{14}$$

So, the total cross sectional area A of a unit cell perpendicular to the flow direction is

$$A = \frac{\pi}{4}\frac{D_\mathrm{f}}{2-D_\mathrm{f}}\frac{1-\varepsilon}{\varepsilon}\lambda_{\max}^2 \tag{15}$$

Thus, the superficial velocity is

$$v_\mathrm{s} = Q/A = \frac{1}{32\mu}\frac{\Delta p_1}{L_0}\frac{2-D_\mathrm{f}}{3+D_\mathrm{T}-D_\mathrm{f}}\frac{\varepsilon}{1-\varepsilon}L_0^{1-D_\mathrm{T}}\lambda_{\max}^{1+D_\mathrm{T}} \tag{16}$$

According to Eq. (16), we can get the pressure drop across the length L_0 along the macroscopic pressure gradient as

$$\frac{\Delta p_1}{L_0} = \frac{32\mu v_\mathrm{s}}{L_0^{1-D_\mathrm{T}}}\frac{3+D_\mathrm{T}-D_\mathrm{f}}{2-D_\mathrm{f}}\frac{1-\varepsilon}{\varepsilon}\frac{1}{\lambda_{\max}^{1+D_\mathrm{T}}} \tag{17}$$

Eq. (17) depicts the pressure drop caused by the viscous energy loss along the flow path. This pressure drop is linearly proportional to the superficial velocity. Eq. (17) is similar to Blake-Kozeny equation, which represents the viscous energy loss. Note that the empirical constant 150 in Blake-Kozeny equation has no physical meaning and is independent of porosity. Whereas every parameter in Eq. (17) has clear physical meaning, and the viscous energy loss expressed by Eq. (17) depends on fluid viscosity, pore size, fluid velocity, porosity, pore area dimension D_f and the tortuosity fractal dimension D_T. However, Blake-Kozeny equation only depends on fluid viscosity, particle size, fluid velocity and porosity, and some other mechanisms (such as pore size distribution described by the fractal dimension D_f and capillary tortuosity described by the fractal dimension D_T) affecting the flow resistance are not revealed. Eq. (17) also indicates that the maximum pose size significantly influences the pressure drop. However, Blake-Kozeny equation does not show this dependence. The following is devoted to deriving a simple model for the maximum pore size.

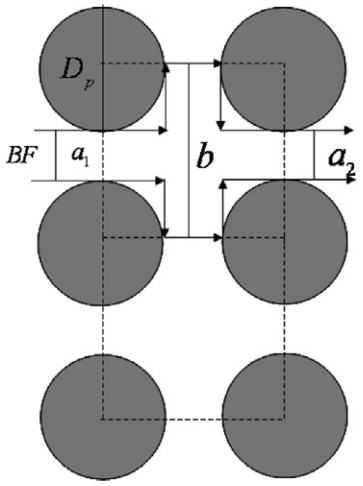

Fig. 1. An idealized pore–throat model.

Based on the idealized pore–throat model as shown in Fig. 1 for flow through porous media, the area of the unit cell is

$$S = \frac{\pi D_\mathrm{p}^2}{4(1-\varepsilon)} \tag{18}$$

The area of the pore is

$$S_{\mathrm{p,max}} = S - \frac{\pi D_\mathrm{p}^2}{4} = \frac{\pi D_\mathrm{p}^2}{4}\left(\frac{1}{(1-\varepsilon)}-1\right) \tag{19}$$

The irregular geometry of the macro-pore area is approximated as a circular pore as

$$S_{\mathrm{p,max}} = \frac{\pi}{4}\lambda_{\max}^2 \tag{20}$$

From Eqs. (19) and (20), $\lambda_{\max}$ can be obtained as

$$\lambda_{\max} = D_\mathrm{p}\sqrt{\frac{\varepsilon}{1-\varepsilon}} \tag{21}$$

Eq. (21) is a simple model for the maximum pore size, which is related to porosity and the equivalent mean diameter D_p. It is evident that if porosity $\varepsilon = 0$, $\lambda_{\max} = 0$; if porosity $\varepsilon = 1$, $\lambda_{\max}$ is infinity. This is consistent with the practical situations. Eq. (21) also indicates that the maximum pore size $\lambda_{\max}$ is proportional to the mean particle diameter D_p. This is also consistent with the physical situation. In Eq. (17), $\lambda_{\max}$ is determined by Eq. (21).

Eq. (17) can also be written as the dimensionless form:

$$G_1 = \frac{\Delta p_1}{L_0}\frac{\rho D_\mathrm{p}^3\varepsilon^3}{\mu^2(1-\varepsilon)^3} = \frac{32}{L_0^{1-D_\mathrm{T}}}\frac{3+D_\mathrm{T}-D_\mathrm{f}}{2-D_\mathrm{f}}\frac{D_\mathrm{p}^2}{\lambda_{\max}^{1+D_\mathrm{T}}}Re_\mathrm{p} \tag{22}$$

where $Re_\mathrm{p} = (D_\mathrm{p}\rho v_\mathrm{s}/\mu)(1-\varepsilon)^{-1}$ is the Reynolds number.

3.2. The kinetic energy loss at high Reynolds numbers

In Fig. 1, the ratio of pore diameter ($BF + D_p = b$) to throat diameter (BF) is defined by β, i.e. $\beta = \frac{BF+D_p}{BF}$, and l is the length of a pore–throat unit. a_1 and a_2 represent the cross sectional areas.

The length of a pore–throat unit is assumed to be $l = b$, and based on Eq. (18), this yields

$$l = b = BF + D_p = \sqrt{S} = D_p\sqrt{\frac{\pi}{4(1-\varepsilon)}} \tag{23}$$

Thus, we obtain

$$BF = D_p\left(\sqrt{\frac{\pi}{4(1-\varepsilon)}} - 1\right) \tag{24}$$

$$\beta = \frac{BF + D_p}{BF} = \frac{1}{1 - 2\sqrt{\frac{(1-\varepsilon)}{\pi}}} \tag{25}$$

Now, we consider the kinetic/local energy loss. The loss of head is expressed by [29]

$$h_f = \sum \xi \frac{\bar{v}_t^2}{2g} \tag{26}$$

where $\bar{v}_t$ is the real average velocity in a throat of cross section area a_1 (see Fig. 1), and ξ represents the coefficient of kinetic/local energy loss. The coefficient for a sudden *expanding* pipe/channel is [29]

$$\xi_e = \left(1 - \frac{a_1}{a}\right)^2 \tag{27}$$

where a is the cross sectional area of the pore. For a sudden *contracting* pipe/channel of cross section area a_2, the coefficient is [29]

$$\xi_c = 0.5\left(1 - \frac{a_2}{a}\right) \tag{28}$$

So, the local loss of head caused by the sudden *expanding* pipe/channel is

$$h_{fe} = \xi_e \frac{\bar{v}_e^2}{2g} = \left(1 - \frac{1}{\beta^2}\right)^2 \frac{\bar{v}_e^2}{2g} \tag{29}$$

and the local loss of head caused by the sudden *contracted* pipe/channel is

$$h_{fc} = 0.5\left(1 - \frac{1}{\beta^2}\right)\frac{\bar{v}_c^2}{2g} = \xi_c \frac{\bar{v}_c^2}{2g} \tag{30}$$

Due to continuity of flow rate, we have

$$q = a_1\bar{v}_e = a_2\bar{v}_c \tag{31}$$

Since $a_1 = a_2$, $\bar{v}_e = \bar{v}_c = \bar{v}_t$. Adding Eqs. (29) and (30) results in the total loss of head

$$h_f = h_{fe} + h_{fc} = (\xi_1 + \xi_2)\frac{\bar{v}_t^2}{2g} = \left(\frac{3}{2} + \frac{1}{\beta^4} - \frac{5}{2\beta^2}\right)\frac{\bar{v}_t^2}{2g} \tag{32}$$

The pressure drop across the pore–throat unit with length l then is

$$\Delta P_2 = \rho g h_f = \left(\frac{3}{2} + \frac{1}{\beta^4} - \frac{5}{2\beta^2}\right)\frac{\rho\bar{v}_t^2}{2} \tag{33}$$

The average velocity in a straight pipe/channel is

$$\bar{v}_0 = \frac{dL_0}{dt} \tag{34}$$

Due to Eq. (9), we can get the relation between average velocity $\bar{v}_t$ in a tortuous capillary and average velocity $\bar{v}_0$ in a straight capillary as follows

$$\bar{v}_t = dL_t/dt = D_T L_0^{(D_T-1)}\bar{\lambda}^{(1-D_T)}\bar{v}_0 \tag{35}$$

Due to overlapping of particles randomly distributed in a porous medium, the fluid passes not only through the maximum macro-pores but also through the narrow channels with the width of BF, and these maximum pores and the narrow channels may be in the same flow direction. Thus, the average pore size $\bar{\lambda}$ in Eq. (35) may be taken as

$$\bar{\lambda} = (\lambda_{max} + BF)/2 \tag{36}$$

Substituting Eqs. (21) and (24) into Eq. (36) yields

$$\bar{\lambda} = \frac{(\lambda_{max} + BF)}{2} = \frac{D_p}{2}\left(\sqrt{\frac{\varepsilon}{1-\varepsilon}} + \sqrt{\frac{\pi}{4(1-\varepsilon)}} - 1\right) \tag{37}$$

Inserting Eq. (35) into Eq. (33) results in

$$\Delta p_2 = \rho g h_f = \left(\frac{3}{2} + \frac{1}{\beta^4} - \frac{5}{2\beta^2}\right)\frac{\rho}{2}\left[D_T L_0^{(D_T-1)}\bar{\lambda}^{(1-D_T)}\right]^2\bar{v}_0^2 \tag{38}$$

Due to the relation between the superficial velocity v_s and the average velocity $\bar{v}_0$, $\bar{v}_0 = v_s/\varepsilon$, Eq. (38) is rewritten as

$$\Delta p_2 = \rho g h_f = \left(\frac{3}{2} + \frac{1}{\beta^4} - \frac{5}{2\beta^2}\right)\frac{\rho v_s^2}{2\varepsilon^2} D_T^2 L_0^{(2D_T-2)}\bar{\lambda}^{(2-2D_T)} \tag{39}$$

Eq. (39) represents the pressure drop along a pore–throat, and the pressure drop per unit length is then

$$\frac{\Delta p_2}{l} = \left(\frac{3}{2} + \frac{1}{\beta^4} - \frac{5}{2\beta^2}\right)\frac{\rho v_s^2}{2\varepsilon^2}\frac{1}{l} D_T^2 L_0^{(2D_T-2)}\bar{\lambda}^{(2-2D_T)} \tag{40}$$

Eq. (40) denotes that the kinetic/local energy loss is linearly proportional to v_s^2, which (v_s) as related to Eq. (16). Eq. (40) represents the kinetic energy loss and is similar to Burke-Plummer equation. However, Burke-Plummer equation contains an empirical constant 1.75, whereas there is no empirical constant in Eq. (40), in which every parameter has clear physical meaning. Eq. (40) is expressed as a function of the pore–throat ratio, porosity, fluid property, pore size, velocity, and fractal dimensions D_f and D_T. While Burke-Plummer equation does not reveal the dependences of the pore–throat ratio, pore size, fractal dimensions D_f and D_T on the pressure drop. Therefore, the physical principles of the kinetic energy loss are clearly revealed in the proposed model Eq. (40).

Eq. (40) can also be expressed in terms of the dimensionless form:

$$G_2 = \frac{\Delta p_2}{l}\frac{\rho D_p^3 \varepsilon^3}{\mu^2(1-\varepsilon)^3} = \left(\frac{3}{2}+\frac{1}{\beta^4}-\frac{5}{2\beta^2}\right)\frac{D_p}{2l}\frac{\varepsilon}{(1-\varepsilon)}D_T^2\left(\frac{L_0}{\bar{\lambda}}\right)^{2D_T-2}Re_p^2 \quad (41)$$

3.3. Total pressure drop

The total pressure drop per unit length is the sum of the viscous energy loss and kinetic/local energy loss along the flow path, i.e.

$$\frac{\Delta p_1}{L_0}+\frac{\Delta p_2}{l} = \frac{32\mu v_s}{L_0^{1-D_T}}\frac{3+D_T-D_f}{2-D_f}\frac{1-\varepsilon}{\varepsilon}\frac{1}{\lambda_{max}^{1+D_T}} + \left(\frac{3}{2}+\frac{1}{\beta^4}-\frac{5}{2\beta^2}\right)\frac{\rho v_s^2}{2\varepsilon^2}\frac{1}{l}D_T^2\left(\frac{L_0}{\bar{\lambda}}\right)^{2D_T-2} \quad (42)$$

Eq. (42) is similar to Ergun equation (1), which has two empirical constants, 150 and 1.75. Whereas there is no empirical constant in Eq. (42) and every parameter in Eq. (42) has the clear physical meaning, and more physical principles are revealed in Eq. (42).

However, in reality, not all the pores/capillaries are spherical, so Eq. (42) is modified by introducing ϕ_s, called sphericity of particles [7], then the modified equation is expressed as

$$\frac{\Delta p_1}{L_0}+\frac{\Delta p_2}{l} = \frac{1}{\phi_s}\frac{32\mu v_s}{L_0^{1-D_T}}\frac{3+D_T-D_f}{2-D_f}\frac{1-\varepsilon}{\varepsilon}\frac{1}{\lambda_{max}^{1+D_T}} + \frac{1}{\phi_s^2}\left(\frac{3}{2}+\frac{1}{\beta^4}-\frac{5}{2\beta^2}\right)\frac{\rho v_s^2}{2\varepsilon^2}\frac{1}{l}D_T^2\left(\frac{L_0}{\bar{\lambda}}\right)^{2D_T-2} \quad (43)$$

where $\phi_s = (36\pi V_P^2/S_P^3)^{1/3}$ [8], here V_P and S_P are volume and surface area of particles, with $\phi_s = 1$ for spherical particles and $\phi_s < 1$ for other shaped particles.

4. Results and discussion

It was generally recognized that the minimum pore size is smaller than the maximum pore size in porous media by at least two orders of magnitude. In this work we thus assume $\lambda_{min}/\lambda_{max} = 10^{-2}$ and $d_{min}/d_{max} = 10^{-2}$. The fractal dimension D for particles can be found by modifying Eq. (8) as

$$D = d_E - \frac{ln(1-\varepsilon)}{\ln(d_{min}/d_{max})}, \quad (44)$$

and the fractal dimension D_T for tortuous capillaries can be obtained from Eq. (9) as

$$D_T = 1 + \frac{\ln\tau}{ln(L_0/\bar{\lambda})} \quad (45)$$

where $\bar{\lambda}$ is determined by Eq. (37), and the tortuosity τ is defined by $\tau = L_t/L_0$ and is expressed as [30]

$$\tau = \frac{1}{2}\left[1+\frac{1}{2}\sqrt{1-\varepsilon}+\sqrt{1-\varepsilon}\frac{\sqrt{\left(\frac{1}{\sqrt{1-\varepsilon}}-1\right)^2+\frac{1}{4}}}{1-\sqrt{1-\varepsilon}}\right] \quad (46)$$

Interested readers may consult reference [30] for the general behavior of the fractal dimension D_T, and for the sensitivity analyses of D_T on the flow resistance/permeability, readers may consult Ref. [21].

Eq. (43) is now rewritten as the dimensionless form,

$$G = G_1 + G_2 = \frac{1}{\phi_s}\frac{32}{L_0^{1-D_T}}\frac{3+D_T-D_f}{2-D_f}\frac{D_p^2}{\lambda_{max}^{1+D_T}}Re_p + \frac{1}{\phi_s^2}\left(\frac{3}{2}+\frac{1}{\beta^4}-\frac{5}{2\beta^2}\right)\frac{D_p}{2l}\frac{\varepsilon}{(1-\varepsilon)}D_T^2\left(\frac{L_0}{\bar{\lambda}}\right)^{2D_T-2}Re_p^2 \quad (47)$$

and Ergun equation is also be rewritten as the dimensionless form, i.e.

$$\frac{\Delta P}{L_0}\frac{\rho D_p^3\varepsilon^3}{\mu^2(1-\varepsilon)^3} = 150Re_p + 1.75Re_p^2 \quad (48)$$

Fig. 2 compares the dimensionless flow resistances predicted respectively by Eqs. (22) and (47) versus Reynolds numbers when $Re_p < 10$ for the spherical particles. The results show that when Reynolds numbers $Re_p < 2.75$, the relative error between the predicted values by the two equations is less than 10%, This means that the pressure drop is mainly determined by the viscous energy loss Eq. (22) at low Reynolds numbers, and Eq. (22) can be a good approximation to the flow resistance at low Reynolds numbers. However, at higher Reynolds numbers, Eq. (47) should be used.

Fig. 3 compares the dimensionless flow resistances predicted respectively by Eqs. (41) and (47) versus the modified Reynolds numbers as $Re_p > 220$. The results show that when the modified Reynolds numbers $Re_p > 220$, the

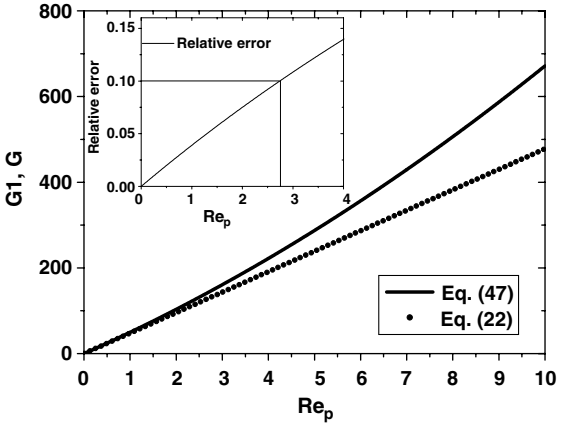

Fig. 2. A comparison on the dimensionless flow resistance versus Re_p at $Re_p < 10$, $\varepsilon = 0.40$, $D_p = 10$ mm.

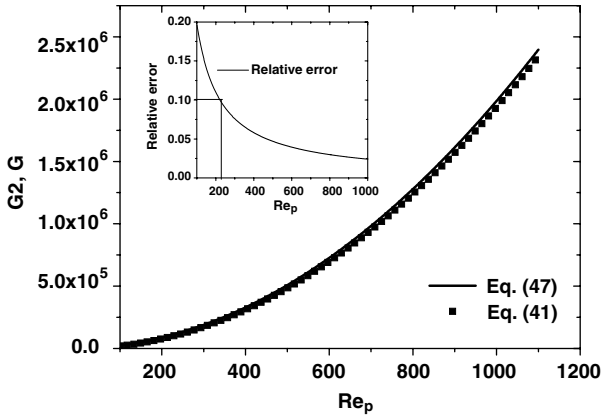

Fig. 3. A comparison on the dimensionless flow resistance versus Re_p at $Re_p > 100$, $\varepsilon = 0.40$, $D_p = 10$ mm.

relative error between the predicted values by the two equations is less than 10%, This means that at high Reynolds numbers the flow resistance is dominated by the kinetic/local energy loss Eq. (41).

It should be noted that Eq. (47) is the general form for resistance of flow through porous media. From Eq. (47) it can be seen that the pressure drop for flow at low speed (or at low Reynolds number) is mainly determined by the viscous energy loss, which is represented by the first term on the right-hand side of Eq. (47). In this case, the irregularity of porous shape can be ignored. At high speed (or at high Reynolds number) the irregularity of porous shapes has the significant influence on flow resistance, and the kinetic/local energy loss dominates the pressure drop, which is mainly determined by the second term on the right-hand side of Eq. (47). Eq. (47) is similar to Ergun equation, which has two empirical constants 150 and 1.75. Whereas there is no empirical constant and every parameter has the clear physical meaning in Eq. (47).

Fig. 4 compares the present model predictions by Eq. (47) with those by Ergun equation (48) and the experiment

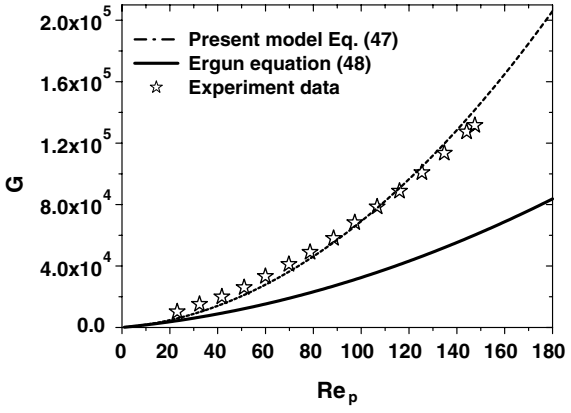

Fig. 4. A comparison among the present model Eq. (47), Ergun equation (48) and experiment data for Quadralobes particles [8] at $\varepsilon = 0.471$, $\phi_s = 0.593$ and $D_p = 1.26$ mm.

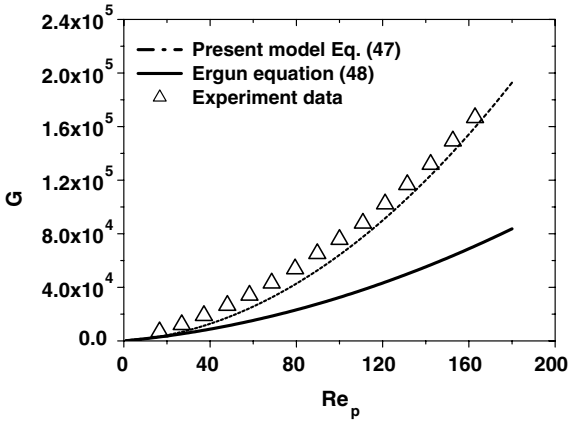

Fig. 5. A comparison among the present model Eq. (47), Ergun equation (48) and experiment data for Trilobes particles [8] at $\varepsilon = 0.511$, $\phi_s = 0.63$ and $D_p = 1.41$ mm.

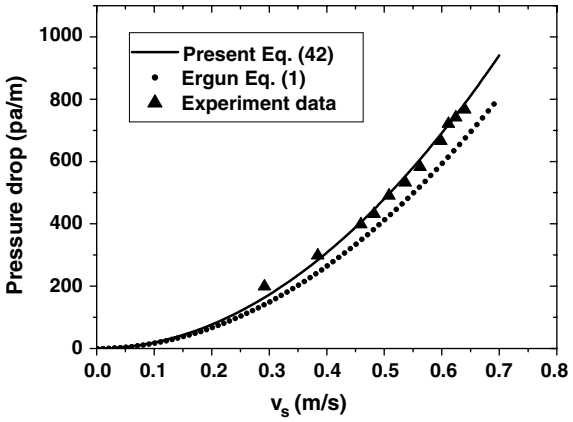

Fig. 6. Pressure drop when air flows through a bed packed with glass balls [31].

data for beds packed with Quadralobes particles [8] of $\phi_s = 0.593$, $D_p = 1.26$ mm at $\varepsilon = 0.502$. Fig. 5 compares the present model predictions by Eq. (47) with those by Ergun equation (48) and the experiment data [8] for beds packed with Trilobes particles of different shapes of $\phi_s = 0.63$, $D_p = 1.41$ mm at $\varepsilon = 0.511$. Fig. 6 compares the present model predictions (at $\varepsilon = 0.433$) by Eq. (42) with those by Ergun equation (1) and the experiment data [31], which were measured for beds packed with spherical particles of $D_p = 10$ mm and $L = 0.5$ m [31], L is the real length of a porous sample. From Figs. 4–6, it can be seen that the model predictions are in good agreement with the experiment data with non-sphericity particles. However, Ergun equation underestimates the resistance, and this may be explained that Ergun equation may only be suitable for spherical particles and for his experimental data.

If Eq. (42) is written as the other dimensionless form, we obtain

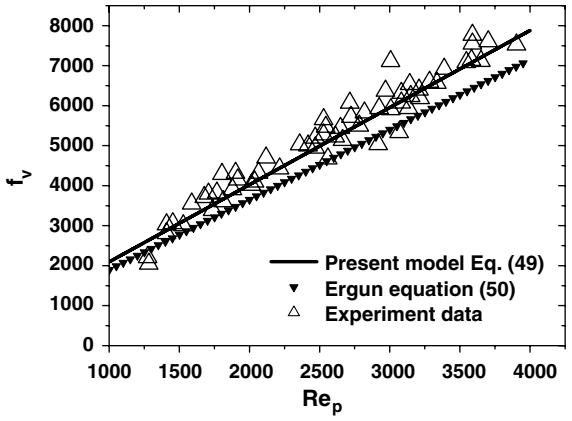

Fig. 7. A comparison among the present model Eq. (49), Ergun equation (50) and experiment data for ball particles [32] at $\varepsilon = 0.364$, $\phi_s = 1$, and $D_p = 12$ mm.

$$f_v = f_{v1} + f_{v2} = \left(\frac{\Delta p_1}{L_0} + \frac{\Delta p_2}{l}\right)\frac{D_p^2\varepsilon^3}{\mu v_s(1-\varepsilon)^2} = \frac{32}{L_0^{1-D_T}}\frac{3+D_T-D_f}{2-D_f}\frac{D_p^2}{\lambda_{max}^{(1+D_T)}} + \left(\frac{3}{2}+\frac{1}{\beta^4}-\frac{5}{2\beta^2}\right)\frac{D_p}{2l} \times \frac{\varepsilon}{(1-\varepsilon)}D_T^2\left(\frac{L_0}{\bar{\lambda}}\right)^{2D_T-2}Re_p \quad (49)$$

Similarly, if Ergun equation (1) is written as the other dimensionless form, we have

$$\frac{\Delta P}{L_0}\frac{D_p^2\varepsilon^3}{\mu v_s(1-\varepsilon)^2} = 150 + 1.75Re_p \quad (50)$$

Fig. 7 compares the present model predictions by Eq. (49) with those by Ergun equation (50) and the experiment data [32] for beds packed with spherical particles of $D_p = 12$ mm, $\varepsilon = 0.364$. From Fig. 7, it can be found that the model predictions also present much better agreement with the experimental data than those by Ergun equation. If Eq. (43) is written as

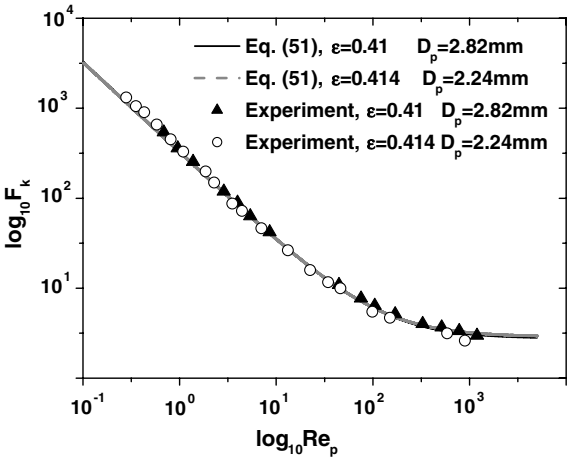

Fig. 8. A comparison of the model predictions with the experimental data by Pahl (1975) [6] at $\varepsilon = 0.41$, $\phi_s = 0.862$ and $\varepsilon = 0.414$, $\phi_s = 0.872$.

$$F_k = \left(\frac{\Delta p_1}{L_0} + \frac{\Delta p_2}{l}\right)\frac{D_p}{\rho v^2}\frac{\varepsilon^3}{(1-\varepsilon)} = \frac{1}{\phi_s^2}\left(\frac{3}{2}+\frac{1}{\beta^4}-\frac{5}{2\beta^2}\right)\frac{D_p}{2l}\frac{\varepsilon}{(1-\varepsilon)}D_T^2\left(\frac{L_0}{\bar{\lambda}}\right)^{2D_T-2} + \frac{1}{\phi_s}\frac{32}{L_0^{1-D_T}}\frac{3+D_T-D_f}{2-D_f}\frac{D_p^2}{\lambda_{max}^{(1+D_T)}}\frac{1}{Re_p} \quad (51)$$

Fig. 8 compares the present model predictions by Eq. (51) with the experiment data [6] for cylindrical particles. From Fig. 8 it can be found that the model predictions also present good agreement with the experimental data.

5. Conclusions

We have shown an analytical model for resistance of fluid flow in porous media based on the capillary model and pore–throat model as well as the fractal characters of pores and capillaries. The proposed model is expressed as a function of the pore–throat ratio, porosity, fluid property, pore/capillary and particle size, fluid velocity (or Reynolds number) and fractal characters (D_f and D_T) of pores and capillaries in porous media. There is no empirical constant and every parameter has clear physical meaning in the proposed model. The physical principles of the viscous energy loss along the flow path and the kinetic energy loss are clearly revealed. The model predictions are compared with experiment data, and good agreement is found between them. The validity of the propose model is thus verified.

It should be pointed out that the accuracy of the present fractal model may crucially depends on the correct determination of sphericity ϕ_s of particles, the maximum pore or particle size, the ratio of $\lambda_{min}/\lambda_{max}$, and the ratio of pore to throat. Therefore, the correct determination of these parameters is critical for successfully predicting the resistance of flow in porous media.

Acknowledgement

This work was supported by the National Natural Science Foundation of China through Grant Number 10572052.

References

[1] S. Ergun, Fluid flow through packed columns, Chem. Eng. Prog. 48 (1952) 89–94.
[2] R.B. Bird, W.E. Stewart, E.N. Lightfoot, Transport Phenomena, Wiley, New York, 1960 (Chapter 6).
[3] R.E. Hicks, Pressure drop in packed beds of spheres, Ind. Eng. Chem. Fund. 9 (1970) 500–502.
[4] R.D. Bradshaw, J.E. Myers, Heat and mass transfer in fixed and fluidized beds of large particles, AIChE. J. 9 (1963) 590–598.
[5] D. Handly, P.J. Heggs, Momentum and heat transfer mechanisms in regular shaped packings, Trans. Inst. Chem. Eng. 46 (1968) 251–259.
[6] F. MacDonald, M.S. Ei-Sayed, K. Mow, F.A.L. Dullien, Flow through porous media—the Ergun equation revised, Ind. Eng. Chem. Fundam. 18 (1979) 199–208.

[7] D. Metha, M.C. Hawley, Wall effect in packed columns, Ind. Eng. Chem., Proc. Des. Dev. 8 (1969) 280–286.
[8] D. Nemec, J. Levec, Flow through packed bed reactors: 1. Single-phase flow, Chem. Eng. Sci. 60 (2005) 6947–6957.
[9] Y. Endo, D-R. Chen, D.Y.H. Pui, Theoretical consideration of permeation resistance of fluid through a particle packed layer, Powder Technol. 124 (2002) 119–126.
[10] R.J. Hill, D.L. Koch, A.J.C. Ladd, Moderate-Reynolds-number flows in ordered and random arrays of spheres, J. Fluid Mech. 448 (2001) 243–278.
[11] B.B. Mandelbrot, The Fractal Geometry of Nature, W.H. Freeman, New York, 1982.
[12] J. Feder, A. Aharony, Fractals in Physics, North-Holland, 1989.
[13] J. Feder, Fractals, Plenum Press, New York, 1988.
[14] T.L. Warren, D. Krajcinovic, Random Cantor set models for the elastic–perfectly plastic contact of roughness surfaces, Wear 196 (1996) 1–15.
[15] F.M. Borodich, A.B. Mosolov, Fractal roughness in contact problems, J. Appl. Math. 56 (1992) 681–690.
[16] A. Majumdar, B. Bhushan, Role of fractal geometry in roughness characterization and contact mechanics of surfaces, J. Tribol. 112 (1990) 205–216.
[17] A.J. Katz, A.H. Thompson, Fractal sandstone pores: implications for conductivity and pore formation, Phys. Rev. Lett. 54 (1985) 1325–1328.
[18] C.E. Krohn, A.H. Thompson, Fractal sandstone pores: automated measurements using scanning-electron-microscope images, Phys. Rev. B 33 (1986) 6366–6374.
[19] B.B. Mandelbrot, D.E. Passoja, A.J. Paullay, Fractal character of fracture surfaces of metals, Nature 308 (1984) 721–722.
[20] H. Xie, R. Bhaskar, J. Li, Generation of fractal models for characterization of pulverized materials, Miner. Metall. Process. (February) (1993) 36–42.
[21] B.M. Yu, P. Cheng, A fractal permeability model for bi-dispersed porous media, Int. J. Heat Mass Transfer 45 (2002) 2983–2993.
[22] B.M. Yu, L.J. Lee, H.Q. Cao, A fractal in-plane permeability model for fabrics, Polym. Compos. 23 (2002) 201–221.
[23] C.O. Karacan, P.M. Halleck, A fractal model for predicting permeability around perforation tunnels using size distribution of fragmented grains, J. Petroleum Sci. Eng. 40 (2003) 159–176.
[24] Y. Shi, J.S. Xiao, M. Pan, Z.R. Yuan, A fractal permeability model for the gas diffusion layer of PEM fuel cells, J. Power Sources 160 (2006) 277–283.
[25] Y. Shi, J.S. Xiao, M. Pan, Z.R. Yuan, Addendum to "A fractal permeability model for gas diffusion layer of PEM fuel cells", J. Power Sources 165 (2007) 299.
[26] F.G. Meng, H.M. Zhang, Y.S. Li, X.W. Zhang, F.G. Yang, Application of fractal permeation model to investigate membrane fouling in membrane bioreactor, J. Membr. Sci. 262 (2005) 107–116.
[27] B.M. Yu, J.H. Li, Some fractal characters of porous media, Fractals 9 (2001) 365–372.
[28] M.M. Denn, Process Fluid Mechanics, Prentice Hall, NJ, 1980.
[29] Y.Y. Zhang, Fluid Mechanics, Higher Education Press, 1999 (Chapters 3 and 6).
[30] B.M. Yu, Fractal character for tortuous streamtubes in porous media, Chin. Phys. Lett. 22 (2005) 158–161.
[31] Z.L. Wang, Y.L. Ding, M. Ghadiri, Flow of a gas–solid two-phase mixture through a packed bed, Chem. Eng. Sci. 59 (2004) 3071–3079.
[32] J. Yu, M.C. Zhang, W.D. Fan, Y.G. Zhou, G.F. Zhao, Study on performance of the ball packed-bed regenerator: experiments and simulation, Appl. Therm. Eng. 22 (2002) 641–651.